The Connection between Microstructural Damage Modeling and Continuum Damage Modeling for Eutectic Sn–Pb Solder Alloys

P. SHARMA
Department of Mechanical Engineering
University of Houston
Houston, TX 77204, USA

A. DASGUPTA* AND G. CUDDALOREPATTA
Department of Mechanical Engineering
University of Maryland
College Park, MD 20742, USA

ABSTRACT: Researchers resort to a wide range of simplified representations at the continuum scale, to model creep–fatigue damage in viscoplastic heterogeneous materials, such as Sn–Pb eutectic solders, caused by thermomechanical and mechanical cyclic loading (e.g., due to power cycling, environmental temperature cycling, vibration, etc.). Typically, in macroscale phenomenological damage models, the cyclic damage is assumed to depend on some loading parameter, such as cyclic strain range, work dissipation per cycle, partitioned strain range, partitioned work dissipation per cycle, cyclic entropy changes, cyclic stress range, integrated matrix creep, etc. In many instances, some of these variables are weighted with a factor to account for rate-dependent effects. The task of finding the best damage metric is difficult because of complex microstructural interactions between cyclic creep and cyclic plasticity due to the high homologous temperature under operating conditions. In this study, we use insights obtained from microstructural and more mechanistic modeling to identify the most appropriate macroscale damage metrics. The microstructural models are based on such phenomena as grain boundary sliding, blocking of grain boundary sliding by second-phase particles, volumetric and grain boundary surface diffusion, void nucleation, void growth, and plastic collapse of cavitating grain boundaries. As has been demonstrated in the literature, micro-

*Author to whom correspondence should be addressed. E-mail: dasgupta@glue.umd.edu

1056-7895/05/04 0343–21 $10.00/0 DOI: 10.1177/1056789505054302

structural models suggest that fatigue damage caused by cyclic plasticity should correlate well with either of the two most commonly used damage indicators: cyclic strain range and plastic work dissipation per cycle. This study, however, demonstrates that in the case of damage dominated by cyclic creep, microstructural models developed by the authors indicate closer correlation of fatigue damage with creep work dissipation per cycle, than with cyclic creep strain range.

KEY WORDS: creep, grain boundary sliding diffusion, void nucleation, void growth, plastic collapse, creep rupture, cyclic loading, microstructural damage model, continuum damage model, eutectic Sn–Pb solder.

INTRODUCTION

FAILURE OF SOLDER interconnects, due to creep–fatigue interactions, is one of the dominant failure modes in surface-mount electronic assemblies, since many solders (such as 63Sn/37Pb) are expected to perform at homologous temperatures well above 0.5 (Frear et al., 1990). The intergranular fracture mode typically observed in solders (as a result of creep-dominated fatigue mechanism) can be accounted for by the following sequence of events: (1) continuous cavity nucleation; (2) cavity growth; and (3) cavity coalescence and interlinkage leading to fracture (e.g., Raj and Ashby, 1975; Edward and Ashby, 1979; Needleman and Rice, 1980; Baik and Raj, 1982; Cocks and Ashby, 1982; Riedel, 1986; Wong and Helling, 1990; Rodriguez and Bhanu Shankara Rao, 1993; Kuo et al., 1995; Giessen and Tvergaard, 1996; Nielsen and Tvergaard, 1998; Onck, 1998). The sequence of damage events described above occurs for both static creep (i.e., creep at constant stress) and cyclic creep (creep-dominated cyclic fatigue).

One can approach the problem of modeling cyclic creep damage from a microscopic perspective (i.e., length scales of the order of grain size) or macroscale (structural level damage modeling). This study mainly focuses on damage modeling at the macroscale but motivated from microscale considerations (i.e., length scale of the grains and microdefects like second-phase particles, cavities, etc.). In addition, one can also classify creep damage models based on the approach taken: e.g., mechanistic versus phenomenological. Mechanistic models are those that make some attempt to represent the physics of the microstructural deformation and damage mechanisms. They are typically used and developed by researchers to obtain better insights into the fundamental mechanisms governing failure of materials. These insights can then be used to either justify existing phenomenological damage models or develop new ones. Phenomenological models are typically used in engineering applications and are based on what is observed empirically. For example, phenomenological macroscale creep–fatigue damage models for solder commonly use damage indicators,

such as total cyclic strain range (Manson, 1965; Coffin, 1971), frequency-modified strain range (Coffin, 1973; Engelmaier, 1983; Shi et al., 2000), partitioned cyclic strain range (Hirschberg and Halford, 1976; Vaynman et al., 1987), cumulative integrated creep strain, and ductility exhaustion (Priest and Ellison, 1981; Hale, 1983; Shine et al., 1984; Shine and Fox, 1987; Knecht and Fox, 1995), total energy dissipated per cycle (Morrow, 1965; Solomon, 1986; Vaynman and Fine, 1991; Darveaux et al., 1995), frequency-modified cyclic energy dissipation (Solomon, 1996), partitioned cyclic energy (Dasgupta et al., 1992; Darbha et al., 2000), entropy per cycle (Basaran and Yan, 1998), instantaneous microstructural state (Frear et al., 1995), crack propagation rates (Wong et al., 1988; Lau, 1990; Sandor, 1990; Pao and Pan, 1990; Attarwala et al., 1992; Rafanelli, 1992; Ross and Liang-Chi, 1994; Syed, 1995), percolation thresholds (Fine et al., 1999; Stolkarts et al., 1999), and other hypothetical 'continuum damage' state variables (Kachanov, 1960; Robotnov, 1969; Leckie and Hayhurst, 1977; Chow and Wang, 1987; Onat and Leckie, 1988; Desai, 1991; Ju et al., 1996; Basaran et al., 1998; Fang et al., 1998; Basaran and Chandaroy, 1999; Qian et al., 1999).

Clearly, the phenomenological and the micromechanics approaches are both important in their own right, although it is obviously desirable to provide a bridge between them such that phenomenological models are developed and refined in accordance with insights obtained from micromechanistic models. Empirically determined damage constants in purely phenomenological models, though useful for design in their limited validity range, are difficult to extrapolate to application situations not included in the initial experimentation. Choice of a macroscale model based on micromechanical considerations may mitigate these risks to some extent as one is reasonably assured that the macroscale model has the right interdependencies between various variables in the damage model. In the subsequent section, the basis for a phenomenological model for eutectic Sn–Pb solder will be established with the help of a micromechanics cyclic creep damage model developed by Dasgupta et al. (2001) and Sharma and Dasgupta (2002a,b).

MICROSTRUCTURAL BASIS FOR A PHENOMENOLOGICAL CYCLIC CREEP DAMAGE MODEL

Details of the micromechanics model are presented elsewhere (Dasgupta et al., 2001; Sharma and Dasgupta, 2002a,b) and are summarized here briefly for completeness. The microscale model is based on the fundamental mechanisms of void nucleation at second-phase particles (Pb islands), void growth, and interlinkage. Only rate-dependent creep failure mechanisms

were considered in the microstructural damage model. The microscale damage model mechanistically includes the effect of particle heterogeneity, grain boundary sliding and its impediment at second-phase particles, diffusional relaxation, grain coarsening, constitutive softening (i.e., effect of progressive damage on constitutive properties), and plastic instability of cavitating grain boundaries.

The microstructural morphology, which needs to be modeled, is shown schematically in Figure 1. An equiaxed Pb island is assumed to be surrounded by a polycrystalline Sn matrix. Some grain boundaries in the Sn matrix intersect with the Pb island. Grain boundaries in the tin matrix slide viscously at high temperatures and when impeded by second-phase Pb particles, generate high local stress concentrations at the particle–matrix interface. At high temperatures, creep mechanisms such as grain boundary diffusion, interfacial and volume diffusion, dislocation glide-climb, and void nucleation, tend to relax the high stress concentrations developed due to blocking of grain boundary sliding.

Microscale Stress History

The microscale stress concentrations are obtained using Eshelby's formalism of eigenstrains (Eshelby, 1957). For simplicity of demonstration, the second-phase particle (Pb phase) is modeled as a spherical inhomogeneity (see Mura, 1987, for detailed definitions of inclusions, inhomogeneities, and eigenstrains) situated at the end of the grain boundaries. The impinging grain boundary is modeled as a cuboidal inclusion with a

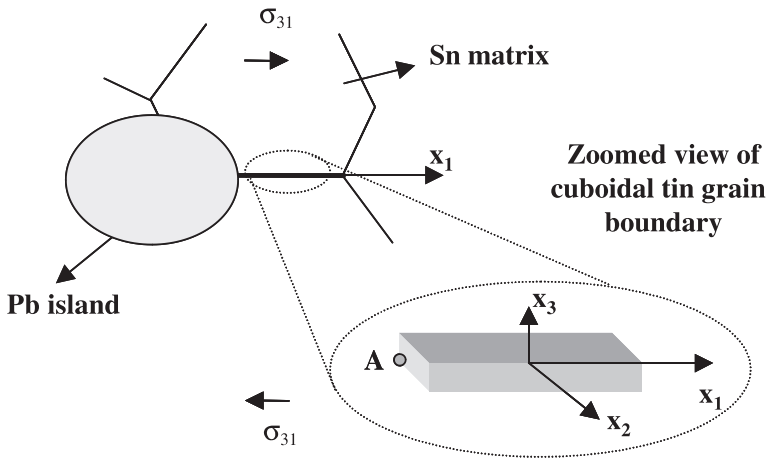

Figure 1. *Idealized geometric configuration of the physical problem.*

prescribed shear eigenstrain (which is equal to the grain boundary sliding strain). The spherical inhomogeneity has a radius 'a' while the cuboidal inclusion has half-lengths a_1, a_2, and a_3. The surrounding matrix is assumed to be isotropic and elastic. This geometric configuration is capable of modeling a wide variety of realistic microstructures. The local stresses at Point A are of primary interest because that is where the highest tensile mean stresses occur and drive void nucleation. The resulting stress field has contributions from: (i) blocking of the grain boundary sliding; and (ii) interactions with the second-phase particle. Thus Eshelby's formalism is an attractive mathematical model for these physical phenomena. As shown elsewhere (Sharma and Dasgupta, 2002a):

$\boldsymbol{\Omega}_e$: (Point A, Figure 1)

$$\begin{aligned}\sigma_{ij} &= C_{ijkl}\left(\varepsilon^{o}_{kl} + S^{e}_{ijkl}\left(\varepsilon^{*}_{kl} + \varepsilon^{R1}_{kl}\right) + D^{c\text{–}A}_{ijkl}\left(\varepsilon^{gbs}_{kl} + \varepsilon^{R2}_{kl}\right) - \varepsilon^{*}_{kl}\right) \\ &= C^{h}_{ijkl}\left(\varepsilon^{o}_{kl} + S^{e}_{ijkl}\left(\varepsilon^{*}_{kl} + \varepsilon^{R1}_{kl}\right) + D^{c\text{–}A}_{ijkl}\left(\varepsilon^{gbs}_{kl} + \varepsilon^{R2}_{kl}\right)\right)\end{aligned} \tag{1}$$

$\boldsymbol{\Omega}_e$ ($x_i = A$) indicates that these equations are solved in the region of the ellipsoid at Point A marked in Figure 1. $\boldsymbol{\varepsilon}^*$ is nonuniform due to the interaction of grain boundary stress field and the inhomogeneity (Moshcovidis and Mura, 1975; Rodin, 1991) and are approximately solved in this study at Point A (Sharma, 2000; Sharma and Dasgupta, 2002a).

Mori et al. (1980) and Onaka et al. (1990) showed that when complete interfacial and long-range volume diffusion takes place, the stress state becomes uniformly hydrostatic and eventually relaxes to the applied stress (i.e., the perturbation due to the inhomogeneity vanishes). In the case of nonuniform stresses found in cuboidal inclusions (Chiu, 1977; Mura, 1987), complete relaxation can occur when $\boldsymbol{\varepsilon}^{R2} + \boldsymbol{\varepsilon}^{gbs} \to 0$ at $t \to \infty$. This discussion can be summarized as follows:

$$\boldsymbol{\varepsilon}^{R1}(t \to \infty) = -\boldsymbol{\varepsilon}^{*}\ (t \to \infty),$$

$$\boldsymbol{\varepsilon}^{R2}(t \to \infty) = -\boldsymbol{\varepsilon}^{gbs}\ (t \to \infty)$$

Strain evolution due to grain boundary sliding (assuming Newtonian viscosity) can be written as (e.g., Chan et al., 1986; Riedel, 1986; Tanaka and Iizuka, 1988):

$$\varepsilon^{gbs}_{31}(t) = -\varepsilon^{max}_{31}\left(1 - e^{-t/tgbs}\right) \tag{2}$$

where, t_{gbs} is the characteristic time for sliding, given as:

$$t_{gbs} = \frac{dkT}{8bD_{bo}\delta_b \exp(-\Delta H/kT)G}\,\phi \tag{3}$$

Here ϕ is an empirical constant and G is the shear modulus. The term ε^{max} is harder to determine however, its upper bound is clearly some fraction of the overall or average creep strain. The formulation in this article will be demonstrated on Sn–Pb eutectic solder. Experiments by Lee and Stone (1994) on solder show that the contribution of grain boundary sliding to the overall strain is nearly 0.25 in the entire range of strain rates within which grain boundary sliding does occur. Further, if far-field stress is held constant, in the long-term limit, the far-field creep strain will reach rupture strains. Thus, in this study, ε^{max} is chosen to be approximately one-fourth of the rupture strain for the given temperature and stress. Since rupture strain also follows a power-law/Arrhenius relationship with respect to temperature and stress, the sliding eigenstrain is given by:

$$\varepsilon^{max} = A_{gbs}\sigma^{m} \exp\left(-\frac{\Delta H_{gbs}}{kT}\right) \tag{4}$$

Within the Pb inhomogeneity, relaxation is governed by the rate of volumetric diffusion. According to Onaka et al. (1990), the volumetric relaxation eigenstrain can be represented as:

$$\varepsilon_{ij}^{R1}(t) = -\varepsilon_{ij}^{*}(1 - e^{-t/t_v}) \tag{5}$$

where t_v is approximately (Onaka et al., 1990):

$$t_v = \frac{kTa^2(3K^h + 4G)}{12GK^h\Omega D_v} \tag{6}$$

The superscript h indicates the inhomogeneity. This approximate expression indicates that the volume diffusion in the Pb-islands is too slow to cause any difference.

The relaxation mechanism within the cuboidal grain boundary due to diffusion also follows first-order kinetics (Mori et al., 1980):

$$\varepsilon_{31}^{R2}(t) = -\varepsilon_{31}^{max}\left(1 - e^{-t/tgbr}\right) \tag{7}$$

where t_{gbr} (characteristic diffusional relaxation time) is (Sharma and Dasgupta, 2002a):

$$t_{gbr} = \frac{kTV_g}{G\Omega D_b \delta_b}\xi \tag{8}$$

ξ (like ϕ) is a local dimensionless geometrical factor, which can only be inferred indirectly from experiments. Note that, all the constants in this model can be obtained from monotonic creep and stress relaxation tests.

Void Nucleation

The microscale stresses, estimated in Equation (1), cause void nucleation. For the purposes of this study, a nucleation rate model, suggested by Giessen and Tvergaard (1990), is modified appropriately:

$$\dot{N} = F_o \frac{N_{max} - N}{N_{max}} \dot{\boldsymbol{\varepsilon}}_c \left(\frac{\sigma_n}{\sigma_o}\right) \qquad \sigma_m > 0 \tag{9}$$

Here, the stresses, strains, and strain rates are to be considered local to the nucleation sites. This nucleation model requires that local σ_m (hydrostatic stress) be positive for nucleation to occur.

Void Growth

Void growth occurs by three mechanisms: grain boundary diffusion (e.g., Hull and Rimmer, 1959; Rice, 1980), power law creep (Budiansky et al., 1982; Tvergaard, 1984), and grain boundary sliding (Sharma, 2000). These rates are:

$$\dot{V}_{diff} = 4\pi \frac{D_b \delta_b \Omega}{kT} \frac{\sigma_b - (1-\omega)\sigma_s}{\ln(1/\omega) - (3-\omega)(1-\omega)/2} \tag{10}$$

$$\dot{V}_{cr} = 2\pi \dot{\varepsilon}_e R^3 h[\alpha_n + \beta_n]^n (\sigma_m/\sigma_e), \qquad (\sigma_m/\sigma_e < 1) \tag{11}$$

$$\dot{V}_{cr} = \mathrm{sgn}(\sigma_m) 2\pi \dot{\varepsilon}_e R^3 h[\alpha_n(\sigma_m/\sigma_e) + \beta_n]^n, \qquad (\sigma_m/\sigma_e > 1) \tag{12}$$

$$\dot{V}_{gbs} = \pi \frac{D_b \delta_b \Omega}{kT} \frac{R}{d} SE\varepsilon_{gbs} \tag{13}$$

The stresses and strain rates are to be considered local to the grain boundary facet, though remote from the cavity (Onck, 1998).

Void Interlinkage

Voids grow and interlink, leading eventually to a macroscale crack. A rigorous mechanistic failure criterion can be established based on the theory of cavitation instability, grain coarsening, progressive degradation of yield strength due to grain coarsening, porosity, and hydrostatic stresses. Details are not presented here as they are quite complicated and the reader is referred to Sharma (2000) for derivations. The input to the void interlinkage models are simply the temperature- and grain size-dependent yield stress, the microstresses, current volume fraction of voids, and the average void spacing (deduced from void nucleation rate and void growth rate).

Cyclic Softening and Grain Coarsening

As the void fraction continues to increase by creep cavitation, the material continues to soften. The Mori–Tanaka (1971) method for estimating average stress in the matrix and in inclusions can be used for computing the change in tangent elastic properties due to void fraction f:

$$\overset{\text{eff}}{C}_{ijkl} = C^{\text{M}}_{klmn}\left\{(1-f)\Delta C_{mnpq}S_{pqrs} + C^{\text{M}}_{mnrs}\right\}^{-1} \left[\Delta C_{rstu}\left\{(1-f)S_{tuij} + f\delta_{tuij}\right\} + C^{\text{M}}_{rsij}\right] \tag{14}$$

For effective creep properties, the Mori–Tanaka method can be extended to nonlinear composites by using the method of Lin (1994):

$$\dot{\varepsilon}_{\text{e}} = \left[\frac{1+0.67f}{(1-f)^n}\right] A\sigma_{\text{e}}^n \exp\left(-\frac{\Delta H}{kT}\right) \tag{15}$$

Grain coarsening affects microstresses, nucleation, void growth, and void linkage and thus must be taken into account explicitly (Upadhyayula, 1999):

$$d^3(t) - d_0^3(t) = \frac{c_1 t}{T}\exp\left(-\frac{\Delta H_{\text{g}}}{RT}\right)\left[1 + \frac{\Delta\sigma}{c_2}\right] \tag{16}$$

In this study, this coarsening law is used incrementally as the temperatures and stress values are continuously changing.

Creep Fatigue Damage Model

The microstructural elements described in Equations (1)–(16) can be combined to form a creep–fatigue damage model. The void radius fraction can be represented by:

$$f_r = \frac{R}{\lambda} \tag{17}$$

As before, R is the void radius while λ is the intervoid half-spacing. The evolution of 'R' occurs as per void growth Equations (10)–(13). The evolution of λ is seen as linked to the nucleation rate. The main effect of continuous nucleation of voids (at a finite rate) is to decrease the average intervoid spacing (Onck, 1998):

$$\lambda = \lambda_o \sqrt{\frac{N_o}{N}} \tag{18}$$

where the subscript 'o' indicates initial values.

Damage is defined as the ratio of the void radius fraction to critical void radius fraction required for cavitation instability:

$$D = \frac{f_r}{f_r^{crit}} \tag{19}$$

f_r^{crit} is estimated based on plastic instability theory, as discussed above in the Section titled ''Void Interlinkage''. The grain size and temperature (which affect yield strength) strongly influence the determination of critical void radius fraction (Sharma and Dasgupta, 2002a). $D = 1$ indicates complete failure. Under compression, where the critical void radius fraction is 1, D is identical to f_r.

This micromechanics-based cyclic creep–fatigue model is implemented in an incremental-iterative manner. The boundary conditions for the micro-scale stress analysis of Section 2.1 are obtained from a global macroscale stress analysis, which is carried out for a given temperature history using any conventional analytical or numerical nonlinear viscoplastic technique. As the material becomes damaged, the macroscale stress-state also changes due to changes in the constitutive properties. As voids grow and interact, the stress field in the tin matrix gets perturbed and alters significantly. These stresses are not appreciably different during the early stages of damage when the void volume fraction is small, however, they contribute significantly at larger void volume fractions (>0.15). In fact, stress disturbances due to

the growing voids are primarily responsible for the acceleration of damage towards the end of the material's life. Evolution of R and λ (and hence the damage D), is tracked throughout the loading history. Based on the current grain size (Equation (16)), yield stress is updated using the Hall–Petch relation and the elastic and creep modulus are updated based on the state of damage. Based on these parameters, the failure surface f_{crit} is also updated. Failure is assumed to occur when the void fraction f reaches the failure locus f_{crit} (i.e., when $D = 1$).

In the following section, sample results of this model are presented, to compare the failure predictions of this microstructural model with predictions based on two commonly used macroscale damage parameters: inelastic cyclic strain range and cyclic work dissipation. Finally, a new phenomenological model is proposed based on the microstructural insights.

RESULTS OF MICROSTRUCTURAL CYCLIC CREEP MODEL

Microstructural failure prediction is based on viscoplastic simulation of all the cycles until failure. The macroscale viscoplastic stress analysis can be computationally too expensive for a complex structure, such as a solder interconnect. Thus, for purposes of illustration in this study, we select a simple structure where the macroscale stresses are uniform and the global analysis can be accomplished semianalytically. The microstructural model is implemented for this idealized structure. Details of the idealized example structure and a sample thermal cycle are given in the Appendix.

Figure 2 shows the growth in void fraction for a typical thermal cycle. Figure 3 shows the decay in the cyclic hysteresis due to softening caused

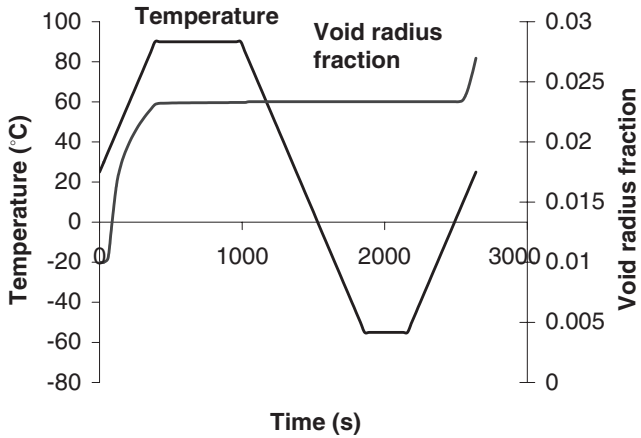

Figure 2. *Void radius fraction evolution in the first cycle for the nominal.*

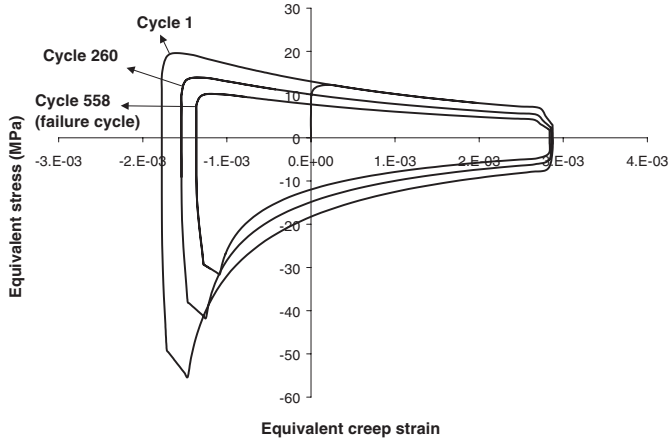

Figure 3. *Progression of cyclic hysteresis loop with damage.*

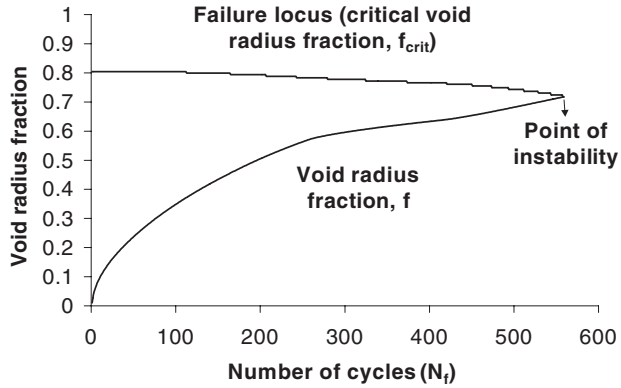

Figure 4. *Void radius fraction and failure locus evolution until complete failure.*

by damage accumulation. Figure 4 shows the corresponding growth in void fraction, decay in failure surface, and ultimate failure due to plastic collapse when the void fraction reaches the critical value. Thus the durability of this structure is obtained for the selected cyclic thermal loading, in terms of cycles to failure.

The next step is to use this microstructural failure prediction to investigate the appropriateness of using traditional phenomenological power-law fatigue models based on macroscale damage parameters, such as the nominal cyclic creep work dissipation and cyclic strain range. Since it is computationally infeasible in a realistic complex structure to simulate all the

cycles to failure, it is common practice to use the 'nominal' value of the macroscale parameters obtained from the initial cycle. In this study, the third cycle is used, as it takes a few cycles to obtain a stable hysteresis loop due to creep and ratchetting. For purposes of comparison, the failure predicted by the microstructural model is plotted against the creep work density and cyclic strain range obtained from the third cycle. The process is repeated for different temperature ranges and ramp rates. Care is taken to ensure that the hydrostatic stress is similar in all cases (to better isolate the relationship between creep work density and cycles-to-failure). The result is shown in Figure 5. To explore if the results are loading-dependent, isothermal stress-controlled cycling is also simulated (at 25 and 70°C) and plotted in Figure 6.

As seen from Figure 5, cycles-to-failure is related to nominal creep work density with a fatigue exponent approximately equal to -1 (i.e., $N_f = AW_c^{-1}$). The small scatter seen at the low-cycle end of the thermal cycling results is due to plotting of several ramp-rate and dwell-time results on the same graph. This scatter suggests that macroscale nominal cyclic creep work density does not capture all the effects that ramp rate and dwell time have on damage accumulation rate (as predicted by the microscale model). It is interesting to note that the exponent is -1 also for slow isothermal mechanical stress cycling. The fact that this slope is not strongly dependent on the type of loading suggests that this model constant can be treated as an intrinsic material property when making phenomenological failure predictions. In Figure 6, when the nominal cyclic strain range is used, the fatigue exponent changes from -1 for isothermal

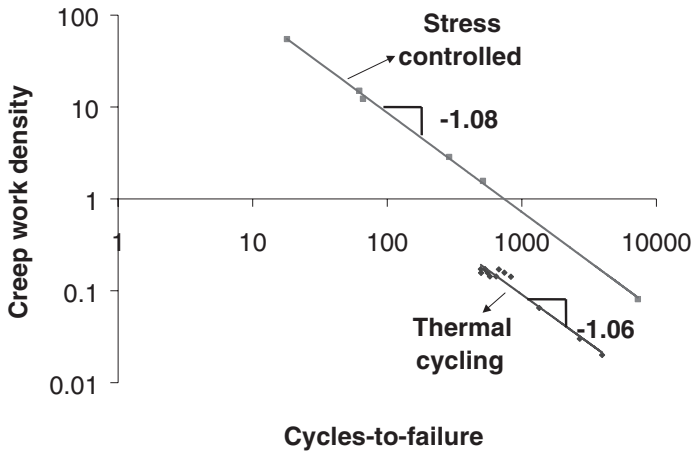

Figure 5. *Creep work density vs cycles-to-failure (microscale predictions).*

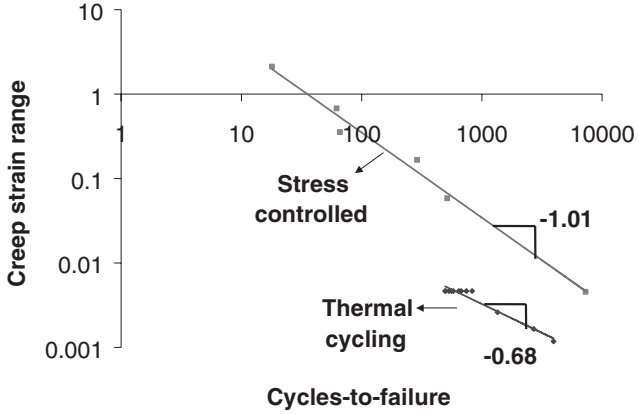

Figure 6. *Creep strain range vs cycles-to-failure (microscale predictions).*

mechanical stress cycling to approximately −0.7 for thermal cycling. Since this model constant changes with the type of loading, it cannot be considered to be an intrinsic material property. Thus, cyclic creep damage is more consistently correlated to the nominal cyclic creep work dissipation than to nominal cyclic strain range, across different types of loading. A macroscale phenomenological model, based on cyclic creep work dissipation, was proposed by Darbha et al. (2000):

$$D = K_2\left(1 - \frac{\sigma_H}{\sigma_F}\right)^{-q} W_c \tag{20}$$

Here, cycles to failure is the reciprocal of the damage D. The fatigue exponent for W_c is −1 in Equation (20), in accordance with the value predicted by the microstructural model in Figure 5. All the model constants are treated as material properties.

The experimentally measured values of the fatigue exponent, which are reported in the literature, have too much scatter, depending on loading conditions and specimen type. Thus it is difficult to see a direct correlation with the predicted values. For example, researchers report the cyclic creep-work fatigue exponent to range from −1 to −1.22 for thermal cycling (Dasgupta et al., 1992; Akay et al., 1997; Jung et al., 1997; Gustafsson, 1998) and from −0.55 to −1.0 for isothermal mechanical strain cycling (Solomon and Tolksdorf, 1995 & 1996; Shi et al., 1999; Haswell, 2001). The corresponding cyclic strain-range fatigue exponent ranges from –0.6 to –1.08 for thermal cycling (Engelmaier, 1983; Sherry and Hall, 1986; Shine et al., 1984) and from −0.55 to −0.7 for isothermal mechanical

strain-cycling (Solomon, 1986; Shi et al., 2000; Haswell, 2001). The strain rates in the mechanical cycling experiments were high enough that the cyclic work and strain-range may have included some plastic contributions in addition to the creep contributions. This adds further complication when comparing test results with model predictions.

PHYSICALLY MOTIVATED MACROSCALE CYCLIC CREEP DAMAGE MODEL – PRELIMINARY EXPLORATION

While the microstructural model shows reasonable correlation to creep-work dissipation, a better macroscale model is proposed here in Equation (21), based on the mechanics embedded in the microstructural model.

$$\dot{D} = K_1 \left(1 + \frac{\sigma_H/\sigma_e}{\Gamma_o}\right)^{n_T} \dot{W}_c \frac{d}{d_{ref}} \tag{21}$$

Here, d_{ref} is a reference grain size. The differences between the proposed model and the energy-partitioning model in Equation (20) are clear. First, the proposed model (henceforth referred to as the energy-rate model or simply the rate model) is explicitly dependent on the loading history (and must be implemented incrementally in time). This model captures the time dependence in the microscale damage model, which the energy-partitioning damage model does not do. Second, this model relies on the triaxiality ratio rather than on the value of the hydrostatic stress, as per insights from the microscale damage model developed by other researchers (e.g., Budiansky et al., 1981) and the present microstructural model (Sharma, 2000). Since, this form is derived from a mechanistic model, we know that the exponent (n_T) is equal to the creep exponent (n_c) for high triaxialities and 1 for low triaxialities. No empirical fitting is necessary any more as was required for q in the energy partitioning model. The linear grain size dependency stems from the fact that creep work at the microscale seems to depend linearly on the grain size (Sharma, 2000).

The model constant K_1 was determined by calibrating the proposed rate model to the results of simple bimetallic structure presented in the Appendix. To test the new model, a case for which experimental results were already available was chosen. Okura (2000) ran detailed experiments on flip chip without underfill. The rate model has to be integrated incrementally along the thermal profile. Special subroutines were written and incorporated in a commercial finite element software (ABAQUS) to implement the rate model. The finite element model built by Okura (2000) was used (Figure 7).

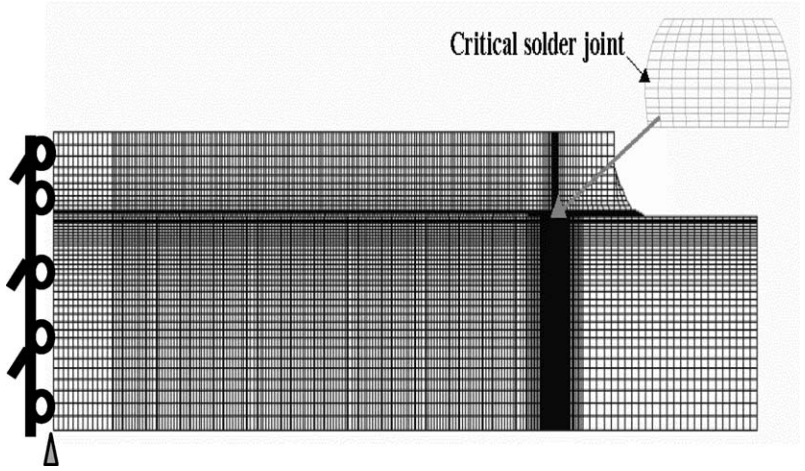

Figure 7. *Finite element model of flip chip without underfill.*

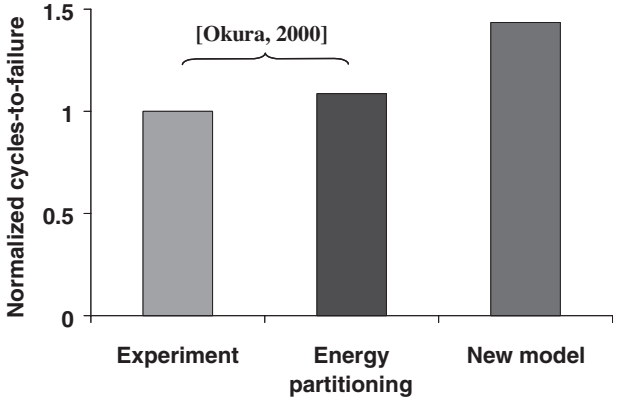

Figure 8. *Comparison of new model with experiments and energy partitioning model.*

The final results of the proposed damage model are compared with the experimental results and the energy-partitioning damage predictions in Figure 8. As can be seen the results are within a scatter band of 1.5. It should be kept in mind that in the proposed damage model no empirical fit was made and all constants were obtained from theoretical (mechanistic) considerations while the energy-partitioning model damage constants were empirically fit. Thus, the proposed model was used in a truly predictive fashion. Furthermore, the proposed model incorporates the physics of the failure process (grain size effect, hydrostatic stress effect, etc.) in a

mechanistic manner and reasonably mimics the trends of the micromechanics model (i.e., the effect of various parameters like ramp rate, dwell time, grain size, etc.) presented elsewhere (Sharma and Dasgupta, 2002a).

CONCLUSIONS

A mechanistic failure model is proposed based on the microstructural phenomena during cyclic creep loading of the solder joints. The microscale model indicates that when formulating macroscale phenomenological failure models, cyclic creep work dissipation is a more consistent damage metric than cyclic strain range. Based on this insight and others obtained from the microscale damage model, a new energy-rate fatigue model is proposed. The model constants of the new cyclic fatigue model are obtained from theoretical considerations and from monotonic creep tests for this material system. When applied to a real solder interconnect (flip chip without underfill), the model agreed with the experimental results within a scatter band of 2. The new model correctly includes the hydrostatic stresses (triaxiality ratio) and is also sensitive to grain size. The proposed model is simple to use and possesses some qualitative features that are rigorously based on mechanistic conclusions, however, more experiments are needed to further validate the model and determine the precise model constants.

APPENDIX

To illustrate the microscale cyclic creep damage model, based on microscale mechanics, a simple but representative case was chosen (Sharma, 2000; Sharma and Dasgupta, 2002a,b). The configuration, as shown in Figure 9,

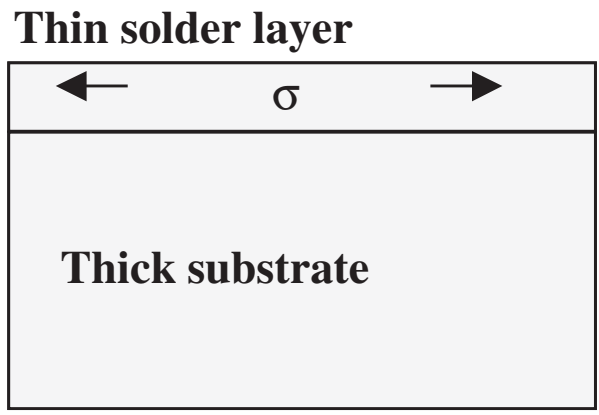

Figure 9. *Global structure.*

consists of a thin layer of solder on a very thick substrate. The substrate is assigned a higher coefficient of thermal expansion (CTE) than solder and thus during a thermal cycle tensile axial stresses will develop in solder during heating and compressive stresses during cooling due to thermal expansion mismatch. The resulting stresses are assumed to be uniformly distributed. In reality, void linkage will occur at different points at different times leading to evolution of a crack. Such an analysis requires the use of an advanced numerical tool like the finite element method. For now, since stresses are assumed to be distributed uniformly, we employ the concept of statistical homogeneity to analyze only a unit cell with a given grain configuration. The grain boundary or the unit cell is assumed to be oriented at an angle of 45° with respect to the direction of uniaxial macrostress. Once failure or void interlinkage occurs in this unit cell, a grain-sized crack is formed. Since the damage is assumed to be uniform, failure in our entire structure will occur at nearly the same time as failure of the unit cell. The 'nominal' loading profile is defined as follows (Table 1). The nominal case has a triaxiality ratio of nearly 0 (actually, it has triaxiality ratio of +0.333 during heating and −0.333 during cooling but since the time spent in the compressive and tensile regimes is not too different we can assume an average triaxiality ratio of 0). The effect of hydrostatic stresses will be studied by imposing an external hydrostatic stress (which will not affect the macroscale stress analysis, as the creep constitutive laws are entirely based on equivalent stress).

For this simplified and idealized structure the global stresses can be found by solving the following differential equation:

$$\Delta\alpha \frac{\mathrm{d}T}{\mathrm{d}t} = \frac{1}{E}\frac{\mathrm{d}\sigma}{\mathrm{d}t} + A\sigma|\sigma|^{n-1}\exp\left(-\frac{\Delta H}{kT}\right) \tag{A1}$$

$\Delta\alpha$ represents the difference in the CTE of the substrate and solder. ΔH is the activation energy for creep, k is Boltzmann's constant while σ is the axial stress developed in solder.

Table 1. Parameters for nominal case.

Temperature range	145°C
Upper temperature	90°C
Ramp up rate	10°C/min
Ramp down rate	10°C/min
Upper dwell time	10 min
Lower dwell time	5 min
CTE of substrate	70 ppm/°C
Thickness of substrate	Very thick
External hydrostatic stress	0
Grain size	3.5 μm

NOMENCLATURE

$\boldsymbol{C}$, $\boldsymbol{C}^{\mathrm{h}}$ = fourth-order elastic stiffness tensor of solder and lead, respectively
$\boldsymbol{\varepsilon}^{\mathrm{o}}$, $\boldsymbol{\varepsilon}^{*}$ = far field or global strain tensor and fictitious eigenstrain tensor, respectively
$\boldsymbol{S}^{\mathrm{e}}$ = Eshelby's tensor for interior points
$\boldsymbol{D}^{\mathrm{c}}$ = Eshelby's tensor for the cuboidal shape (for exterior points)
A = superscript 'A' indicates that the cuboidal Eshelby's tensor is evaluated at Point A
$\boldsymbol{\varepsilon}^{\mathrm{R1}}$, $\boldsymbol{\varepsilon}^{\mathrm{R2}}$ = eigenstrains representing volume and interfacial diffusion, respectively
Ω = atomic volume
k = Boltzmann's constant
d = grain size
$D_{\mathrm{b}}\delta_{\mathrm{b}}$ = grain boundary and thickness coefficient
S = shape factor (gbs void-growth model)
σ_{n} = local normal stress at particle–matrix interface
$\varepsilon_{\mathrm{c}}/\varepsilon_{\mathrm{e}}$ = equivalent strain or creep strain
F_{o} = model constant for nucleation model
σ_{o} = normalization constant in nucleation model
$N_{\max}$ = max number of nucleation sites per unit grain boundary area
N = instantaneous number of nucleation sites per unit grain boundary area
N_{o} = initial number of nucleation sites per unit grain boundary area
ϕ = shape factor used in relaxation equation
h = shape factor to calculate void volume (assuming spherical caps geometry; see Riedel, 1987)
ξ = shape factor used in relaxation equations
λ = intervoid half spacing
R = void radius

REFERENCES

Akay, H., Zhang, H. and Paydar, N. (1997). *Advances in Electronic Packaging, INTERpack'97*, **2**: 1583–1592.

Attarwala, A.I., Tien, J.K., Masada, G.Y. and Dody, G. (1992). *Trans. of ASME Journal of Electronic Packaging*, **114**(2): 109–111.

Baik, S. and Raj, R. (1982). *Metallurgical Transactions A (Physical Metallurgy and Materials Science)*, **13A**(7): 1207–1214.

Basaran, C. and Chandaroy, R. (1999). *ASME Trans. Journal of Electronic Packaging*, **121**: 8–12.

Basaran, C., Desai, C.S. and Kundu, T. (1998). *ASME Trans. Journal of Electronic Packaging*, **120**: 41–47.

Basaran, C. and Yan, C.Y. (1998). A Damage Criterion Based on Entropy for Pb40/Sn60 Solder Alloys, In: *ASME, Int. Mechanical Engineering Congress and Exposition*, Anaheim, CA, November 15–20, 1998.

Budiansky, B., Hutchinson, J.W. and Slutsky, S. (1982). Void Growth and Collapse in Viscous Solids, In: Hopkins, H.G. and Sewell, M.J. (eds), *Mechanics of Solids*, The Rodney Hill 60th Anniversary Volume, Pergamon Press, Oxford.

Chan, K.S., Page, R.A. and Lankford, J. (1986). *Acta Metalurgica*, **34**: 2361–2370.

Chiu, Y.P. (1977). *J. of Applied Mechanics*, **44**: 587–590.

Chow, C.L. and Wang, J. (1987). *Engineering Fracture Mechanics*, **27**(5): 547–558.

Cocks, A.C.F. and Ashby, M.F. (1982). *Progress in Material Science*, **27**: 189–244.

Coffin, L.F. (1971). *Journal of Materials*, **6**(2): 388–402.

Coffin, L.F. (1973). *ASTM STP*, **520**: 112.

Darbha, K., Okura, J.H., Shetty, S., Dasgupta, A., Reinikainen, T., Zhu, J. and Caers, J.F.J.M. (2000). *Transactions of the ASME. Journal of Electronic Packaging*, **121**(4): 237–241.

Darveaux, R., Banerji, K., Mawer, A. and Dody, G. (1995). Reliability of Plastic Ball Grid Array Assembly, In: Lau, J. (ed.), *Ball Grid Array Technology*, McGraw Hill, Inc., New York.

Dasgupta, A., Oyan, C., Barker, D. and Pecht, M. (1992). *ASME Trans. Electronic Packaging*, **144**: 152–160.

Dasgupta, A., Sharma, P. and Upadhyayula, K. (2001). *International Journal of Damage Mechanics*, **10**(2): 101–132.

Desai, C.S. (1991). *3rd International Conference on Constitutive Laws for Engineering Materials: Theory and Applications*, Tuscon, Arizona.

Edward, G.H. and Ashby, M.F. (1979). *Acta Metallurgica*, **27**(9): 1505–1518.

Engelmaier, W. April 1983. *Electronic Packaging Production*, pp. 58–63.

Eshelby, J.D. (1957). *Proc. Royal. Soc.*, **A241**: 376–396.

Fang, H.E., Chow, C.L. and Yang, F. (1998). *Key Engineering Materials (Switzerland)*, **145–149**(pt.1): 367–374.

Fine, M.E., Stolkarts, V. and Keer, L.M. (1999). *Materials Science and Engineering A (Structural Materials: Properties, Microstructure and Processing)*, **A272**(1): 5–9.

Frear, D., Jones, W.B. and Kinsman, K.R. (eds) (1990). *Solder Mechanics: A State of the Art Assessment*, TMS Publications.

Frear, D.R., Burchett, S.N. and Rashid, M.M. (1995). Advances in Electronic Packaging 1995, In: *Proceedings of the International Electronic Packaging Conference – INTERpack '95*, Vol. 1, pp. 347–360.

Giessen, E.V.D. and Tvergaard, V. (1990). In: Wilshire, B. and Evans, R.W. (eds), *Creep and Fracture of Engineering Materials and Structures*, Elsevier, Swansea.

Giessen, E.V.D. and Tvergaard, V. (1996). *Acta Materiala*, **44**: 2697–2709.

Gustafsson, G. (1998). *Electronic Components and Technology Conference*, pp. 87–91.

Hale, R. (1983). *Fatigue of Engineering Materials and Structures*, **6**(2): 121–135.

Haswell, P. (2001). Durability Assessment and Microstructural Observations of Selected Solder Alloys, PhD Dissertation, Dept. of Mechanical Engineering, University of Maryland, College Park, MD.

Hirschberg, M.H. and Halford, G.R. (1976). *NASA Technical Note*, D-8072.

Hull, D. and Rimmer, D.E. (1959). *Philosophical Magazine*, **4**: 673–687.

Ju, S.W., Sandor, B. and Plesha, M.E. (1996). *Journal of Testing and Evaluation*, **24**(6): 411–418.

Jung, W., Lau, J.H. and Pao, Y.H. (1997). *NEPCON West '97*, 1076–1095.

Kachanov, L.M. (1960). *The Theory of Creep*, English translation by A.J. Kennedy, Boston Spa, Wetherby.

Knecht, S. and Fox, L. (1995). In: Lau, J. (ed.), *Solder Joint Reliability – Theory and Applications*, Van Nostrand Reinhold, NY.

Kuo, C.G., Sastry, S.M.L. and Jerina, K.L. (1995). *Metallurgical and Materials Transactions A*, **26A**: 3625–3275.

Leckie, F.A. and Hayhurst, D.R. (1977). *Acta Metallurgica*, **25**(9): 1059–1070.

Lau, J. (1990). *Solder Joint Reliability: Theory and Application*, Van Nostrand Reinhold, NY.

Lee, S.M. and Stone, D.S. (1994). *Scripta Metallurgica et Materiala*, **30**: 1213–1218.

Lin, S.C. (1994). The Equivalent Inclusion Method in Elasticity and Composite Materials, PhD Dissertation, Northwestern University, Illinois.

Manson, S.S. (1965). *Experimental Mechanics*, **5**: 193–226.

Mori, T., Okabe, M. and Mura, T. (1980). *Acta Metallurgica*, **28**: 319–325.

Mori, T. and Tanaka, K. (1973). *Acta Metallurgica*, **21**(5): 571–574.

Morrow, J.D. (1965). *Internal Friction, Damping and Cyclic Plasticity, ASTM-STP 378*, Warrendale, PA, pp. 45–87.

Moshcovidis, Z.A. and Mura, T. (1975). *J. of Appl. Mech.*, **42**: 847–852.

Mura, T. (1987). *Micromechanics of Defects in Solids*.

Needleman, A. and Rice, J.R. (1980). *Acta Metallurgica*, **28**: 1315–1332.

Nielsen, H.S. and Tvergaard, V. (1998). *International Journal of Damage Mechanics*, **7**(1): 3–23.

Okura, J.H. (2000). Effects of Temperature and Moisture on Durability of Low Cost Flip Chip on Board (FCOB) Assemblies, PhD Dissertation, University of Maryland, College Park, MD.

Onaka, S., Miura, S. and Kato, M. (1990). *Mechanics of Materials*, **8**: 285–292.

Onat, E.T. and Leckie, F.A. (1988). *Transactions of the ASME. Journal of Applied Mechanics*, **55**(1): 1–10.

Onck, P.R. (1998). High-temperature Fracture of Polycrystalline Materials, PhD Dissertation, Technical University of Delft, Netherlands.

Pao, Y.H. and Pan, Tsung-Yu (1990). *Transactions of the ASME. Journal of Electronic Packaging*, **112**(2): 154–161.

Priest, R.H. and Ellison, E.G. (1981). *Materials Science and Engineering*, **49**: 7–17.

Qian, Z., Ren, W. and Liu, S. (1999). *Transactions of the ASME. Journal of Electronic Packaging*, **121**(3): 162–168.

Rafanelli, A.J. (1992). *Transactions of the ASME. Journal of Electronic Packaging*, **114**(2): 234–238.

Raj, R. and Ashby, M.F. (1975). *Acta Metallurgica*, **23**: 653–666.

Rice, J.R. (1980). In: Nemat-Nasser (ed.), *Proceedings of the IUTAM Symposium*, pp. 173–184.

Riedel, H. (1986). *Fracture at High Temperature*, Springer-Verlag, Heidelberg, Germany.

Rodin, G.J. (1991). *Int. J. Solids Structures*, **27**: 145–159.

Rodin, G.J. and Hwang, Y.-L. (1991). *International Journal of Solids and Structures*, **27**(2): 145–159.

Rodriguez, P. and Bhanu Sankara Rao, K. (1993). *Progress in Materials Science*, **37**(5): 403–480.

Ross, R.G., Jr. and Liang-Chi, W. (1994). *Transactions of the ASME. Journal of Electronic Packaging*, **116**(2): 69–75.

Sandor, B. (1990). In: Frear, D.R., Jones, W.B. and Kinsman, K.R. (eds), *Solder Mechanics: A State of the Art Assessment*, Chapter 8, TMS.

Sharma, P. (2000). Microstructural Modeling of Cyclic Creep Damage in Tin-Lead Eutectic Solder, PhD Dissertation, Dept. of Mechanical Engineering, University of Maryland, College Park, MD.

Sharma, P. and Dasgupta, A. (2002a). *ASME Journal of Electronic Packaging*, **124**: 292–297.

Sharma, P. and Dasgupta, A. (2002b). *ASME Journal of Electronic Packaging*, **124**: 298–304.

Sherry, W.M. and Hall, P.M. (1986). In: Fellbach, W. (ed.), *Proc. Conf. Interconnection Technology in Electronics*, Germany, Deutscher Verband fur Schweisstechnik, pp. 47–61.

Shi, X.Q., Pang, H.I.J., Zhou, W. and Wang, Z.P. (1999). *Scripta Materiala*, **41**(3): 289–296.

Shi, X.Q., Pang, H.I.J., Zhou, W. and Wang, Z.P. (2000). *International Journal of Fatigue*, **22**(3): 217–228.

Shine, M.C., Fox, L.R. and Sofia, J.W. (1984). *Proceedings of the International Packaging Society*, **4**: 346.

Shine, M.C. and Fox, L.R. (1987–1988). *ASTM STP942*, 588.

Solomon, H.D. (1986). *IEEE Trans. CHMT*, **9**(4): 423–432.

Solomon, H.D. and Tolksdorf, E.D. (1995). *Trans. of ASME Journal of Electronic Packaging*, **117**: 130–135.

Solomon, H.D. and Tolksdorf, E.D. (1996). *Trans. of ASME Journal of Electronic Packaging*, **118**: 67–71.

Stolkarts, V., Keer, L.M. and Fine, M.E. (1999). *Journal of the Mechanics and Physics of Solids*, **47**(12): 2451–2468.

Syed, A.R. (1995). *Transactions of the ASME. Journal of Electronic Packaging*, **117**(2): 116–122.

Tanaka, M. and Iizuka, H. (1988). In: Solomon, H.D., Halford, G.R., Kaisand, L.R. and Leis, B.N. (eds), *Low Cycle Fatigue, ASTM STP 942*, pp. 611–621, ASTM, Philadelphia.

Tvergaard, V. (1984). *Journal of Mechanics of Physics of Solids*, **32**: 373–393.

Upadhyayula, K. (1999). Incremental Damage Superposition Approach for Surface Mount Electronic Interconnect Durability under Combined Temperature and Vibration Environments, PhD Thesis, University of Maryland, College Park, MD.

Vaynman, S., Fine, M.E. and Jeanotte, D.A. (1987). *TMS-AIME Symposium on Effect of Load and Thermal Histories on Mechanical Behavior of Materials.*

Vaynman, S. and Fine, M.E. (1991). In: Lau, J. and Reinhold, Van Nostrand (eds), *Solder Joint Reliability: Theory and Application*, Chapter 11.

Wong, B., Helling, D.E. and Clark, R.W. (1988). *IEEE Transactions on Components, Hybrids, and Manufacturing Technology*, **11**(3): 284–290.

Wong, B. and Helling, D.E. (1990). *Journal of Electronic Packaging, Transaction of the ASME*, **112**: 104–109.